Electronic Supplementary Material (ESI) for Nanoscale.

Heterostructures Engineering of Co doped MoS_2 coupling with Mo_2CT_x MXene for Enhanced Hydrogen Evolution in Alkaline Media

Junmei Liang, Chaoying Ding, Jiapeng Liu, Tao Chen, WenChao Peng, Yang Li, Fengbao Zhang and Xiaobin Fan*

School of Chemical Engineering and Technology, State Key Laboratory of Chemical Engineering, Collaborative Innovation Center of Chemical Science and Engineering, Tianjin University, Tianjin 300072, China

E-mail: xiaobinfan@tju.edu.cn

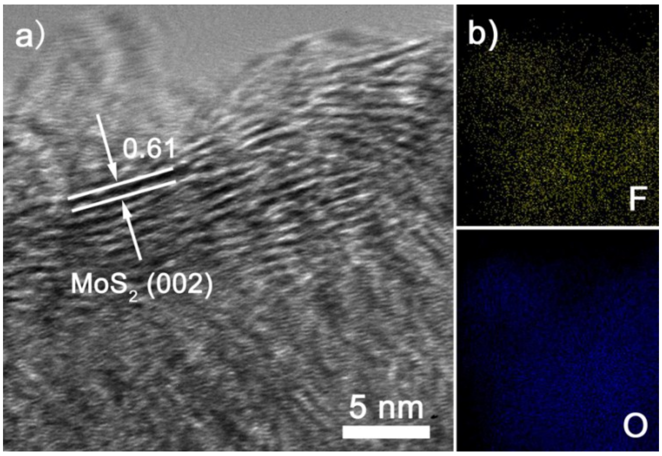

Figure S1 a) HRTEM image of pristine MoS_2; b) elemental mapping showing the uniform distribution of F and O elements in Co-MoS_2/Mo_2CT_x nanohybrids.

The following simplified reactions occurs when the exfoliation of $M_{n+1}AX_n$ phase by HF solution, the as-obtained pristine MXene are chemically terminated with oxygen-containing and/or fluoride functional groups. Thus, the negatively charged terminal groups (–F and –O) can be detected by elemental mapping.

$$M_{n+1}AX_n + 3HF = AF_3 + M_{n+1}X_n + 1.5H_2 \qquad (1)$$

$$M_{n+1}X_n + 2H_2O = M_{n+1}X_n(OH)_2 + H_2 \qquad (2)$$

$$M_{n+1}X_n + 2HF = M_{n+1}X_nF_2 + H_2 \qquad (3)$$

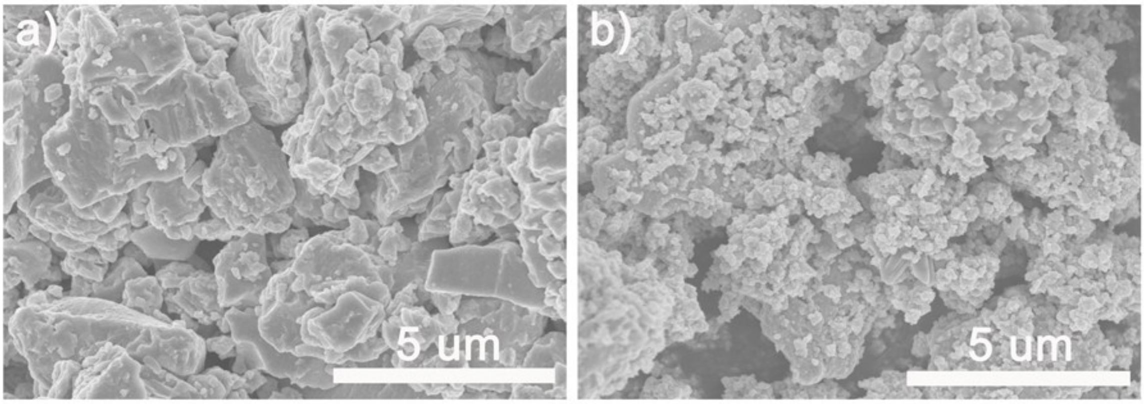

Figure S2 SEM images of a) pure MoS_2 and b) Co-MoS_2/Mo_2CT_x nanohybrids.

The SEM images of pure MoS_2 and Co-MoS_2/Mo_2CT_x nanohybrids have been shown in Figure S2. The pure MoS_2 in Figure S2a shows the large bulk morphology, while the Co-MoS_2/Mo_2CT_x nanohybrid in Figure S2b exhibits dispersed MoS_2 particles attached on the surface of Mo_2CT_x MXene. This result further confirms the Mo_2CT_x MXene can prevent MoS_2 particles from agglomeration during preparation progress. The corresponding modification is also made in original manuscript.

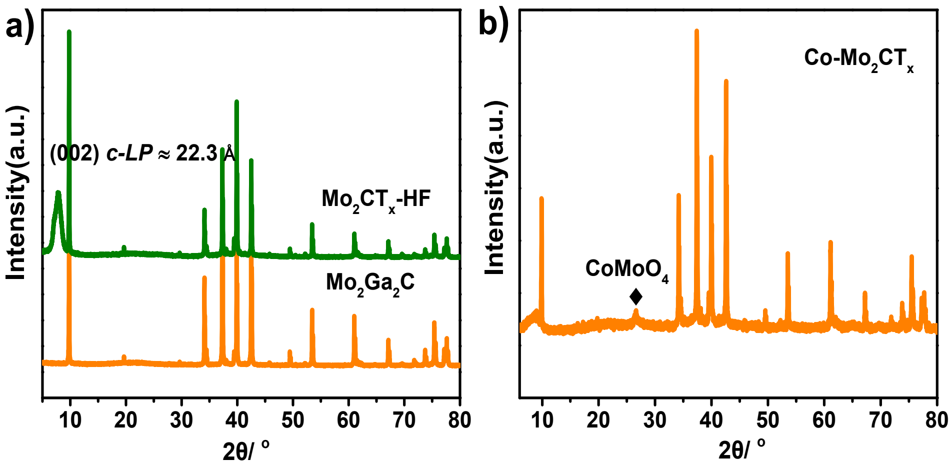

Figure S3 a) XRD patterns of Mo_2CT_x MXene by HF etching without annealing in Ar atmosphere and pristine Mo_2Ga_2C; b) XRD pattern of Co-Mo_2CT_x sample.

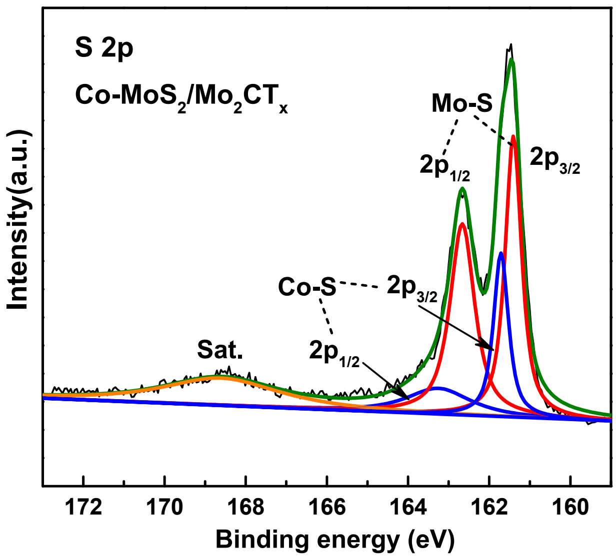

Figure S4 XPS spectrum of S 2p in Co-MoS_2/Mo_2CT_x hybrid.

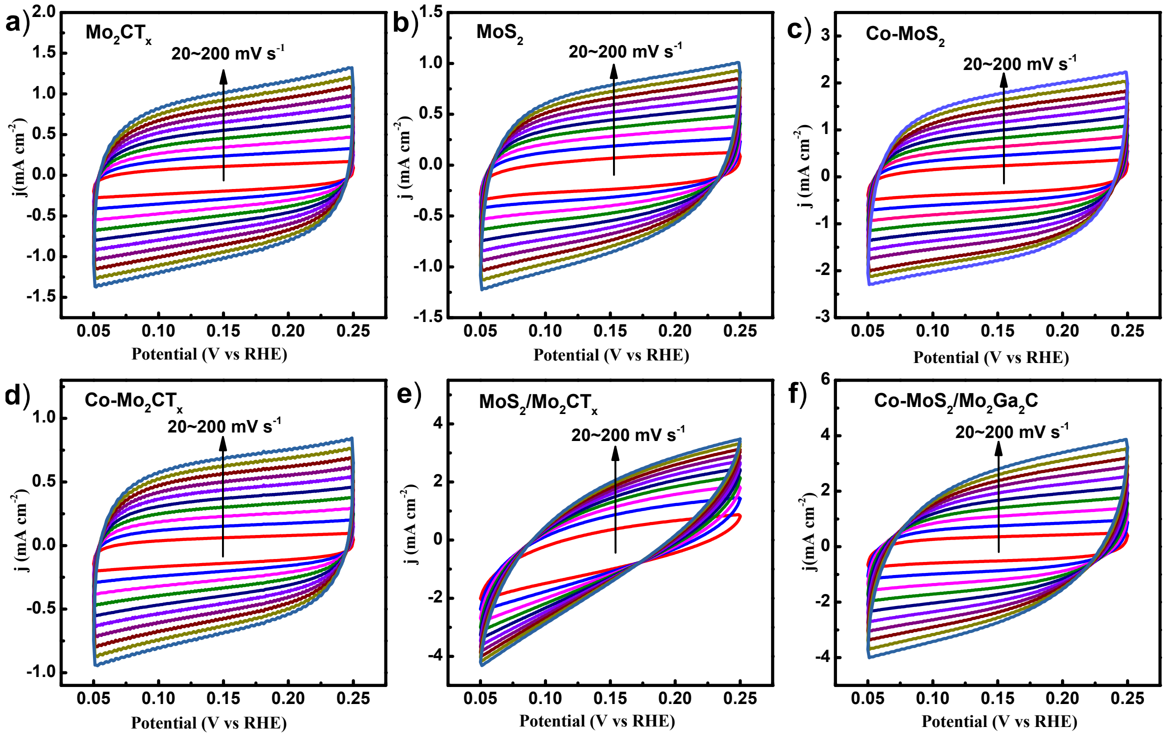

Figure S5 Cyclic voltammograms for different materials at the different rates range from 20 to 200 mV s^{-1}.

To evaluate the electrochemically active surface area (ECSA), a series of cyclic voltammetry (CV) measurements were performed at different scan rates varying from 20 to 200 mV s^{-1} in the region from 0.05 to 0.25 V to determine the double-layer capacitance (C_{dl}). For comparison, the CV at different scan rates of Co-MoS_2/Mo_2Ga_2C catalyst was performed. The results are shown in **Figure S5**.

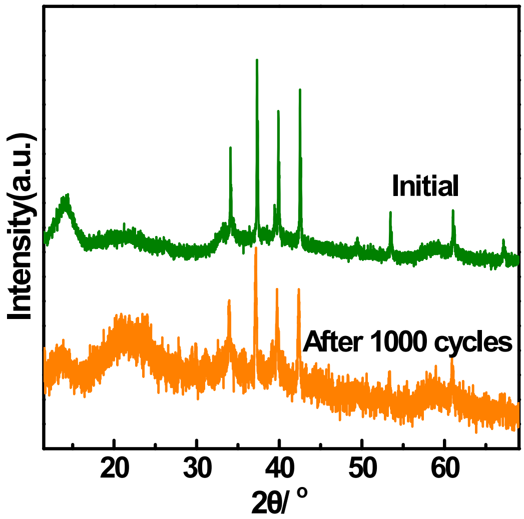

Figure S6 XRD patterns of Co-MoS_2/Mo_2CT_x catalyst before and after stability test.

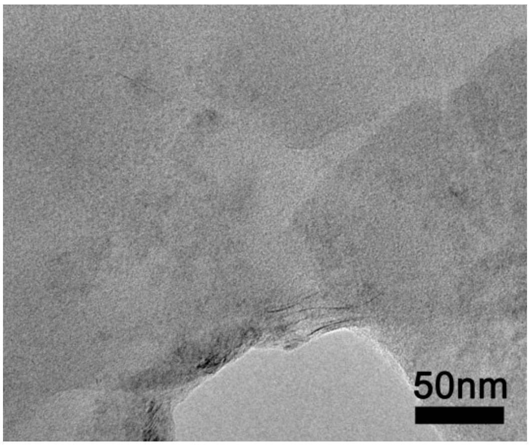

Figure S7 TEM image of Co-MoS_2/Mo_2CT_x after stability test.

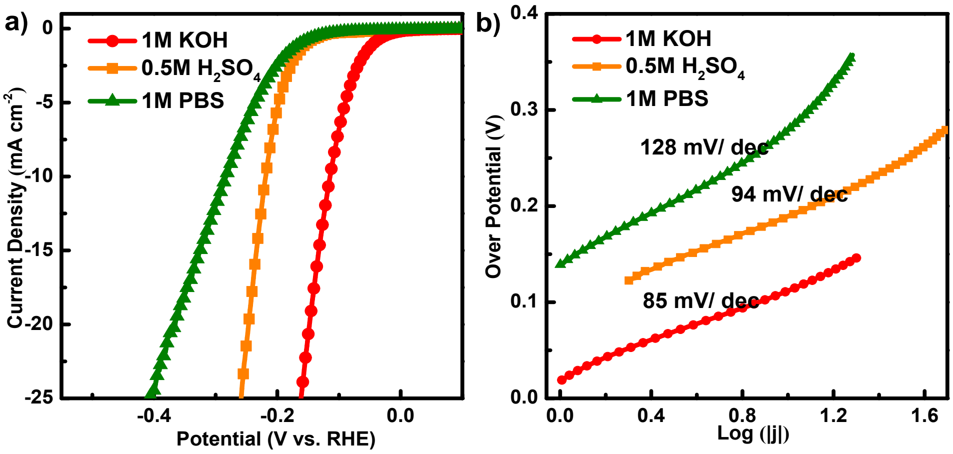

Figure S8 a) Polarization curves of Co-MoS_2/Mo_2CT_x in 1M KOH, 0.5 M H_2SO_4 and 1M PBS electrolytes and b) the corresponding Tafel plots.

The HER performance of Co-MoS_2/Mo_2CT_x electrode in acid and neutral media were evaluated and the results are compared in Figure S8. The Co-MoS_2/Mo_2CT_x electrocatalyst exhibits the small overpotentials of 218 and 286 mV at current density of 10 mA cm^{-2} in acid and neutral media, respectively. Accordingly, the Tafel slopes are 94 and 128 mV dec^{-1} in acid and basic media. The results suggest the great potential of all pH hydrogen evolution for Co-MoS_2/Mo_2CT_x hybrids. In addition, the Co-MoS_2/Mo_2CT_x electrocatalyst exhibits much better alkaline HER activity than acidic HER activity, suggesting the enhanced HER activity of Co-MoS_2/Mo_2CT_x catalyst in alkaline media is mainly attributed to the initially accelerated water dissociation, rather than the hydrogen adsorption properties.

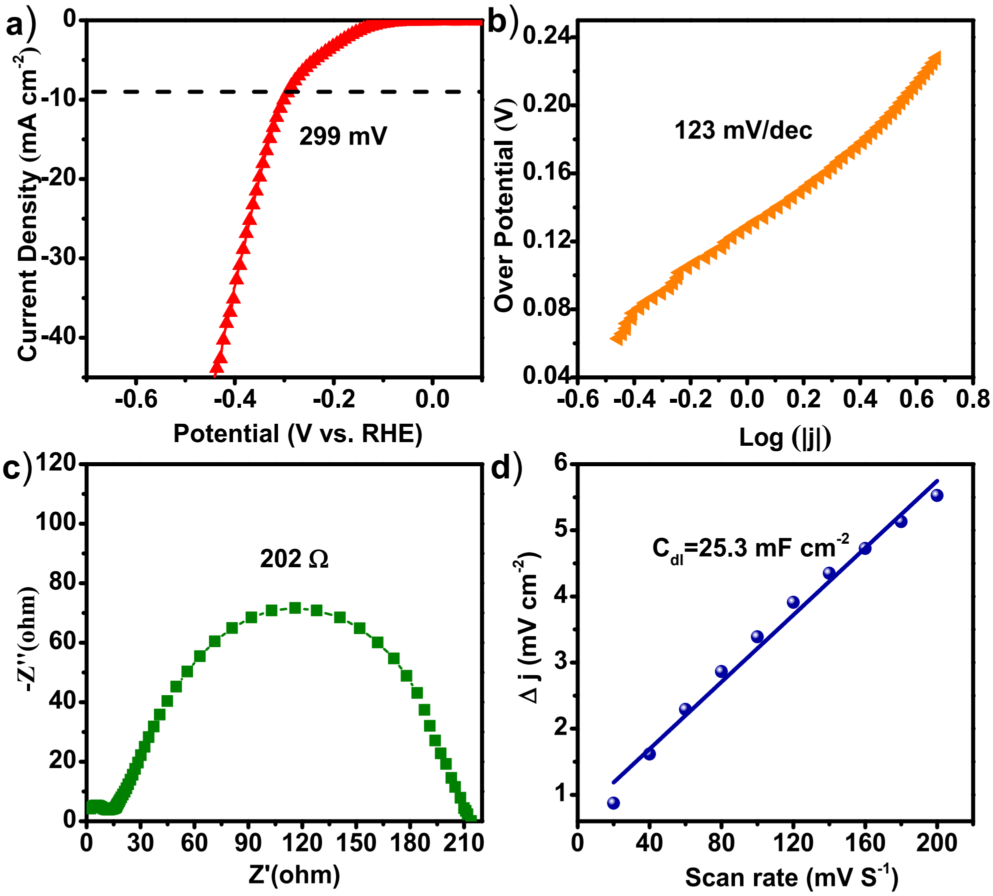

Figure S9 a) Polarization curves of Co-MoS_2/Mo_2Ga_2C catalyst at a scan rate of 5 mV s^{-1} in 1 M KOH; b) Tafel plots of Co-MoS_2/Mo_2Ga_2C catalyst; c) EIS spectrum of Co-MoS_2/Mo_2Ga_2C catalyst at η = 200 mV; d) capacitive current at 0.15 V as a function of scan rates (20 to 200 mV s^{-1}) for Co-MoS_2/Mo_2Ga_2C catalyst.

In view of the effect of etching by HF solution, the HER performance of Co-MoS_2/Mo_2Ga_2C catalyst was evaluated, and the results are shown in **Figure S9**. It suggests Co-MoS_2/Mo_2Ga_2C exhibits lower HER activity than Co-MoS_2/Mo_2CT_x catalyst.

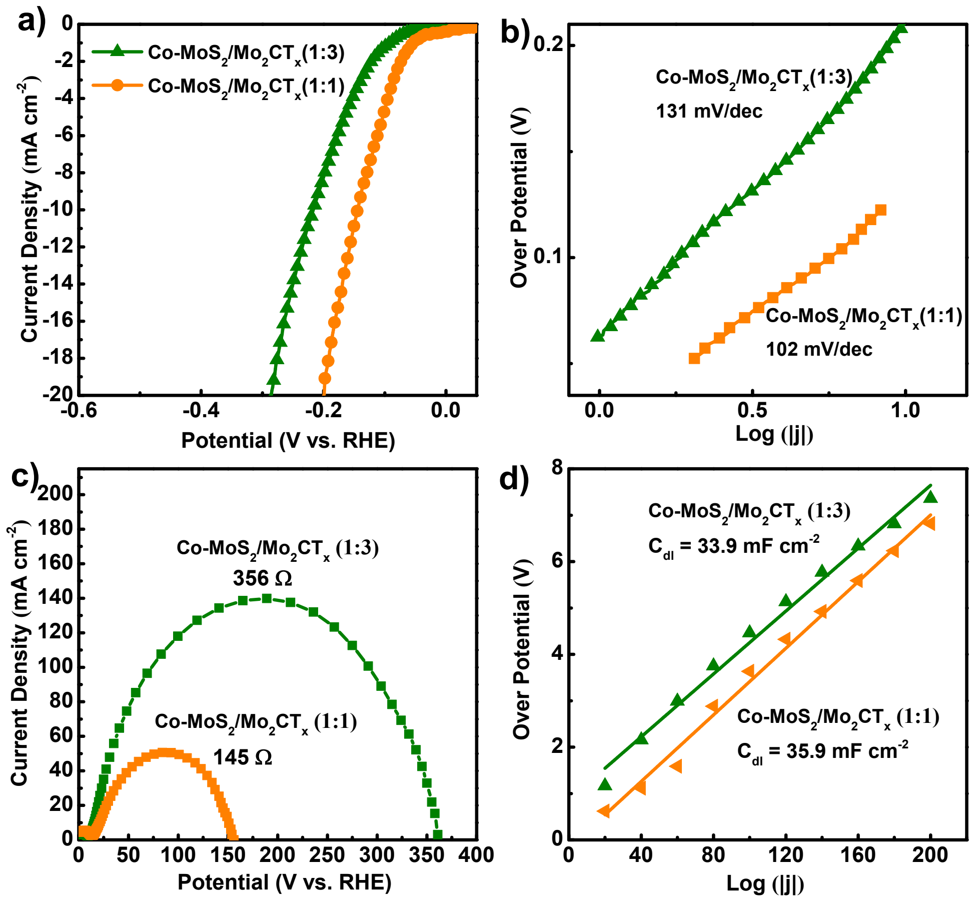

Figure S10 a) Polarization curves, b) Tafel plots, c) EIS spectra and d) capacitive current at 0.15 V as a function of scan rates (20 to 200 mV s^{-1}) of Co-MoS_2/Mo_2CT_x catalyst at different ATTM/Mo_2CT_x mass ratios.

The HER performance of Co-MoS_2/Mo_2CT_x strongly depends on ATTM/Mo_2CT_x mass ratios. The ATTM/Mo_2CT_x MXene mass ratio of 3:1 described in manuscript displays higher HER activity than ATTM/Mo_2CT_x MXene mass ratio of 1:1 and 1:3.

Table S1 A comparison of Co-MoS_2/Mo_2CT_x electrocatalyst with recently reported non-noble metal catalysts in HER performance (1M KOH).

Catalysts	Overpotential at j = 10 mA cm^{-2} (mV)	Tafel slope (mV dec^{-1})	References	Cites
Co-MoS_2/Mo_2CT_x	**112**	**82**	**This work**	
Ni/Mo_2C-PC	179	101	*Chem. Sci.*, 2017, **8**, 968	1
MoS_2/Ti_3C_2-MXene@C	135	45	*Adv. Mater.*, 2017, **29**, 1607017	2
Mo_2C-C	149	66	*Nano Energy*, 2017,**32**, 511–519	3
Cu@NiFe LDH	116	58.9	*Energy Environ. Sci.*, 2017, **10**, 1820	4
Co-MoS_2	163	158	*Energy Environ. Sci.*,2016*,* ***9,*** *2789*	5
CoMoO-S/NF	134	87	*J. Catal.*, 2018*,* **361**, 204–213	6
MoSSe	140	40	*Adv. Mater.*, 2018, **30**, 1705509	7
NC@$CuCo_2N_x$/CF	105	76	*Adv. Funct. Mater.*, 2017, **27**, 1704169	8
Ti_2CT_x nanosheets	170	100	*Nano Energy*, 2018*,* **47***, 512–518*	9
NiCu@C-1	74	94.5	*Adv. Energy Mater.*, 2018, **8**, 1701759	10
CuCoO-NWs	140	108	*Adv. Funct. Mater.*, 2016, **26**, 8555–8561	11
CoP@NC-NG	155	68.6	*Small*, 2017,**14**,702895	12
$CoSe_2$	200	85	*Adv. Mater.*, 2016, **28,** 7527	13
R-MoS_2@NF	71	100	*Adv. Mater.*, 2018, **30**, 1707105	14
SWCNTs/$MoSe_2$	170	67	*Adv. Energy Mater.*, 2018, **8**, 1703212	15

Supplementary References

1. Z. Y. Yu, Y. Duan, M. R. Gao, C. C. Lang, Y. R. Zheng and S. H. Yu, *Chem Sci*, 2017, **8**, 968-973.
2. X. Wu, Z. Wang, M. Yu, L. Xiu and J. Qiu, *Adv. Mater.*, 2017, **29**, 1607017.
3. Z. Wu, J. Wang, R. Liu, K. Xia, C. Xuan, J. Guo, W. Lei and D. Wang, *Nano Energy*, 2017, **32**, 511-519.
4. L. Yu, H. Zhou, J. Sun, F. Qin, F. Yu, J. Bao, Y. Yu, S. Chen and Z. Ren, *Energy Environ. Sci.*, 2017, **10**, 1820-1827.
5. J. Zhang, T. Wang, P. Liu, S. Liu, R. Dong, X. Zhuang, M. Chen and X. Feng, *Energy Environ. Sci.*, 2016, **9**, 2789-2793.
6. Z.-Z. Liu, X. Shang, B. Dong and Chai， Yong-Ming, *J. Catal.*, 2018, **361** 204-213.
7. C. Tan, Z. Luo, A. Chaturvedi, Y. Cai, Y. Du, Y. Gong, Y. Huang, Z. Lai, X. Zhang, L. Zheng, X. Qi, M. H. Goh, J. Wang, S. Han, X. J. Wu, L. Gu, C. Kloc and H. Zhang, *Adv. Mater.*, 2018, **30**, 1705509.
8. J. Zheng, X. Chen, X. Zhong, S. Li, T. Liu, G. Zhuang, X. Li, S. Deng, D. Mei and J.-G. Wang, *Adv. Funct. Mater.*, 2018, **27**, 1704169.
9. S. Li, P. Tuo, J. Xie, X. Zhang, J. Xu, J. Bao, B. Pan and Y. Xie, *Nano Energy*, 2018, **47**, 512-518.
10. Y. Shen, Y. Zhou, D. Wang, X. Wu, J. Li and J. Xi, *Adv. Energy Mater.*, 2018, **8**, 1701759.
11. M. Kuang, P. Han, Q. Wang, J. Li and G. Zheng, *Adv. Funct. Mater*, 2016, **26**, 8555-8561.
12. J. Ma, M. Wang, G. Lei, G. Zhang, F. Zhang, W. Peng, X. Fan and Y. Li, *Small*, 2018, **14**, 1702895.
13. P. Chen, K. Xu, S. Tao, T. Zhou, Y. Tong, H. Ding, L. Zhang, W. Chu, C. Wu and Y. Xie, *Adv. Mater.*, 2016, **28**, 7527-7532.
14. M. A. R. Anjum, H. Y. Jeong, M. H. Lee, H. S. Shin and J. S. Lee, *Adv. Mater.*, 2018, **30**, 1707105.
15. L. Najafi, S. Bellani, R. Oropesa-Nuñez, A. Ansaldo, M. Prato, A. E. Del Rio Castillo and F. Bonaccorso, *Adv. Energy Mater.*, 2018, **8**, 1703212.